

A Short Course on Topological Insulators

J. K. Asbóth, L. Oroszlány, A. Pályi

September 14, 2021

These lecture notes provide an introduction to some of the main concepts of topological insulators, a branch of solid state physics that is developing at a fast pace. They are based on a one-semester course for MSc and PhD students at the Eötvös University, Budapest, which the authors have been giving since 2012.

Our aim is to provide an understanding of the core topics of topological insulators – edge states, bulk topological invariants, bulk–boundary correspondence – with as simple mathematical tools as possible. We restricted our attention to one- and two-dimensional band insulators. We use noninteracting lattice models of topological insulators, and build these up gradually to arrive from the simplest one-dimensional case (the Su-Schrieffer-Heeger model for polyacetylene) to two-dimensional time-reversal invariant topological insulators (the Bernevig-Hughes-Zhang model for HgTe). In each case we introduce the model first, discuss its properties, and then generalize. The prerequisite for the reader is quantum mechanics and not much else: solid state physics background is provided as we go along.

Since this is an introduction, rather than a broad overview, we try to be self-contained and give citations to the current literature only where it is absolutely necessary. For a broad overview, including pointers to the original papers and current topics, we refer the reader to review articles and books in the Introduction.

Supporting material for these lecture notes in the form of ipython notebooks will be made available online.

Despite our efforts, the book inevitably contains typos, errors, and less comprehensible explanations. We would appreciate if you could inform us of any of those; please send your comments to janos.asboth@wigner.mta.hu.

Acknowledgments. We are grateful for enlightening discussions on topological insulators with Anton Akhmerov, Andrea Alberti, Carlo Beenakker, and Alberto Cortijo. We thank the feedback we got from participants at the courses at Eötvös University, especially Vilmos Kocsis. A version of this course was given by one of us (J.K.A.) in the PhD programme of the University of Geneva, on invitation by Markus Büttiker, which helped shape the course.

The preparation of the first version of these lecture notes were supported by the grant TÁMOP4.1.2.A/1-11/0064. We acknowledge financial support from the Hungarian Scientific Research Fund (OTKA), Grant Nos. PD100373, K108676, NN109651, and from the Marie Curie programme of the European Union, Grant No. CIG-293834. J.K.A. and A.P. were supported by the János Bolyai Scholarship of the Hungarian Academy of Sciences

Budapest,
September 2015

János K. Asbóth, László Oroszlány, András Pályi

Introduction

The band theory of electric conduction was one of the early victories of quantum mechanics in the 1920s. It gave a simple explanation of how some crystalline materials are electric insulators, even though electrons in them can hop from one atom to the next. In the bulk of a band insulator, the electrons occupy eigenstates that form energy bands. In a band insulator, there are no partially filled bands: completely filled bands are separated by an energy gap from completely empty bands, the gap represents the energy cost of mobilizing electrons. In contrast, materials with partially filled bands are conductors, where there are plane wave states available to transmit electrons across the bulk at arbitrarily low energy. Although we now know of situations where band theory is inadequate (e.g., for Mott insulators), it remains one of the cornerstones of solid states physics.

The discovery of the Quantum Hall Effect (1980) has shown that the simple division into band insulators and metals is not the end of the story, not even in band theory. In the quantum Hall effect, a strong magnetic field confines the motion of electrons in the bulk, but the same field forces them into delocalized edge states on the surface. A two-dimensional metal in strong magnetic field is thus an insulator in the bulk, but conducts along the surface, via a discrete number of completely open edge state channels (in the language of the Landauer–Büttiker formalism). The number of edge state channels was linked to the Chern number, a topological invariant of the occupied bands (1982).

Over the last twenty years, theoretical progress over artificial systems has shown that the external magnetic field is not necessary for an insulator to have robust conducting edge states: instead, the nontrivial topology of the occupied bands is the crucial ingredient. The name *topological insulator* was coined for such systems, and their study became a blossoming branch of solid state physics. Following the theoretical prediction (Bernevig, Hughes and Zhang, 2006 [5]), electronic transport measurements confirmed that a thin layer of HgTe is a topological insulator (König et al, 2007 [21]). Since that time, a host of materials have been shown to be three-dimensional topological insulators, and thin films and quantum wires shown to be two- and one-dimensional topological insulators [2].

The intense theoretical interest in topological insulators has led to signature results, such as the so-called periodic table of topological insulators [29], which shows that similarly to phase transitions in statistical mechanics, it is the dimensionality and the basic symmetries of an insulator that decide whether it can be a topological insulator or not. Although it was derived by different ways of connecting topological insulators of various dimensions and symmetries (so-called dimensional reduction schemes), the

mathematically rigorous proof of the periodic table is still missing.

The field of topological insulators is very active, with many experimental challenges and open theoretical problems, regarding the effects of electron-electron interaction, extra crystalline symmetries, coupling to the environment, etc.

Literature

To get a quick and broad overview of topological insulators, with citations for relevant research papers, we recommend the review papers [17, 25, 7]. For a more in-depth look, there are already a few textbooks on the subject (by Bernevig and Hughes [4], by Shen [30], and one edited by Franz and Molenkamp [10]). To see the link between momentum-space topology and physics in a broader context, we direct the reader to a book by Volovik[34].

There are also introductory courses on topological insulators with a broad scope. We recommend the lectures by Charles Kane (the video recording of the version given at Veldhoven is freely available online), and the online EdX course on topology in condensed matter by a group of lecturers, with the corresponding material collected at topocondmat.org.

These lecture notes

Our aim with this set of lecture notes is to complement the literature cited above: we wish to provide a close look at some of the core concepts of topological insulators with as simple mathematical tools as possible. Using one- and two-dimensional noninteracting lattice models, we explain what edge states and what bulk topological invariants are, how the two are linked (this is known as the *bulk–boundary correspondence*), the meaning and impact of some of the fundamental symmetries.

To keep things as simple as possible, throughout the course we use noninteracting models for solid state systems. These are described using single-particle lattice Hamiltonians, with the zero of the energy corresponding to the Fermi energy. We use natural units, with $\hbar = 1$ and length measured by the lattice constant.

Contents

1	The Su-Schrieffer-Heeger (SSH) Model	1
1.1	The SSH Hamiltonian	1
1.2	Bulk Hamiltonian	3
1.3	Edge States	6
1.4	Chiral Symmetry	9
1.5	Number of Edge States as Topological Invariant	15
1.6	Summary	20
	Problems	21
2	Berry Phase, Chern Number	23
2.1	Discrete Case	23
2.2	Continuum Case	27
2.3	Berry Phase and Adiabatic Dynamics	32
2.4	Berry's Formulas for the Berry Curvature	34
2.5	Example: The Two-Level System	35
2.6	Graphical Methods to Determine the Chern Number in Two-Band Models	39
2.7	Summary	41
	Problems	42
3	Polarization and Berry Phase	43
3.1	The Rice-Mele Model	44
3.2	Wannier States in the Rice-Mele Model	44
3.3	Inversion Symmetry and Polarization	48
	Problems	50
4	Adiabatic Charge Pumping, Rice-Mele Model	51
4.1	Charge Pumping in a Control Freak Way	52
4.2	Moving Away from the Control Freak Limit	55
4.3	Tracking the Charges with Wannier States	60
	Problems	64

5	Current Operator and Particle Pumping	65
5.1	Particle Current at a Cross Section of the Lattice	66
5.2	Time Evolution Governed by a Quasi-Adiabatic Hamiltonian	71
5.3	The Pumped Current Is the Berry Curvature	75
	Problems	78
6	Two-Dimensional Chern Insulators: The Qi-Wu-Zhang Model	79
6.1	Dimensional Extension: From an Adiabatic Pump to a Chern Insulator	80
6.2	Edge States	84
6.3	Robustness of edge states	91
	Problems	93
7	Continuum Model of Localized States at a Domain Wall	95
7.1	One-Dimensional Monatomic Chain in an Electric Potential	96
7.2	The SSH Model and the One-Dimensional Dirac Equation	100
7.3	The QWZ Model and the Two-Dimensional Dirac Equation	106
	Problems	111
8	Time-Reversal Symmetric Two-Dimensional Topological Insulators: The Bernevig–Hughes–Zhang Model	113
8.1	Time-Reversal Symmetry	114
8.2	Doubling the Hilbert Space for Time-Reversal Symmetry	119
8.3	A Concrete Example: The Bernevig-Hughes-Zhang Model	120
8.4	Edge States in Two-Dimensional Time-Reversal Invariant Insulators .	121
8.5	Absence of Backscattering	124
9	The \mathbb{Z}_2 Invariant of Two-Dimensional Topological Insulators	133
9.1	Tools: Nonabelian Berry Phase, Multiband Wannier States	134
9.2	Time-Reversal Restrictions on Wannier Centers	138
9.3	Two Types of Wannier Center Flow	140
9.4	The \mathbb{Z}_2 Invariant for Systems with Inversion Symmetry	142
	Problems	144
10	Electrical Conduction of Edge States	145
10.1	Electrical Conduction in a Clean Quantum Wire	146
10.2	Phase-Coherent Electrical Conduction in the Presence of Scatterers . .	148
10.3	Electrical Conduction in Two-Dimensional Topological Insulators . .	149
10.4	An Experiment with HgTe Quantum Wells	152

Chapter 1

The Su-Schrieffer-Heeger (SSH) Model

We take a hands-on approach and get to know the basic concepts of topological insulators via a concrete system: the Su-Schrieffer-Heeger (SSH) model describes spinless fermions hopping on a one-dimensional lattice with staggered hopping amplitudes. Using the SSH model, we introduce the concepts of the single-particle Hamiltonian, the difference between bulk and boundary, chiral symmetry, adiabatic equivalence, topological invariants, and bulk–boundary correspondence.

1.1 The SSH Hamiltonian

The Su-Schrieffer-Heeger (SSH) model describes electrons hopping on a chain (one-dimensional lattice), with staggered hopping amplitudes, as shown in Fig. 1.1. The chain consists of N unit cells, each unit cell hosting two sites, one on sublattice A , and one on sublattice B . Interactions between the electrons are neglected, and so the dynamics of each electron is described by a single-particle Hamiltonian, of the form

$$\hat{H} = v \sum_{m=1}^N (|m, B\rangle \langle m, A| + h.c.) + w \sum_{m=1}^{N-1} (|m+1, A\rangle \langle m, B| + h.c.). \quad (1.1)$$

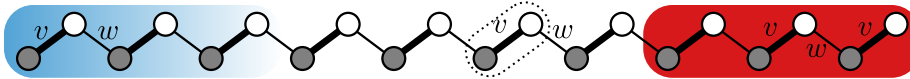


Figure 1.1: Geometry of the SSH model. Filled (empty) circles are sites on sublattice A (B), each hosting a single state. They are grouped into unit cells: the $m = 6$ th cell is circled by a dotted line. Hopping amplitudes are staggered: intracell hopping v (thick lines) is different from intercell hopping w (thin lines). The left and right edge regions are indicated by blue and red shaded background.

Here $|m, A\rangle$ and $|m, B\rangle$, with $m \in \{1, 2, \dots, N\}$, denote the state of the chain where the electron is on unit cell m , in the site on sublattice A , respectively, B , and *h.c.* stands for Hermitian Conjugate (e.g., *h.c.* of $z|m, B\rangle\langle m, A|$ is $z^*|m, A\rangle\langle m, B|$ for arbitrary $z \in \mathbb{C}$).

The spin degree of freedom is completely absent from the SSH model, since no term in the Hamiltonian acts on spin. Thus, the SSH model describes spin-polarized electrons, and when applying the model to a real physical system, e.g., polyacetylene, we have to always take two copies of it. In this chapter we will just consider a single copy, and call the particles fermions, or electrons, or just particles.

We are interested in the dynamics of fermions in and around the ground state of the SSH model at zero temperature and zero chemical potential, where all negative energy eigenstates of the Hamiltonian are singly occupied (because of the Pauli principle). As we will show later, due to the absence of onsite potential terms, there are N such occupied states. This situation—called half filling—is characteristic of the simplest insulators such as polyacetylene, where each carbon atom brings one conduction electron, and so we find one particle (of each spin type) per unit cell.

For simplicity, we take the hopping amplitudes to be real and nonnegative, $v, w \geq 0$. If this was not the case, if they carried phases, $v = |v|e^{i\phi_v}$, and $w = |w|e^{i\phi_w}$, with $\phi_v, \phi_w \in [0, \pi)$, these phases could always be gauged away. This is done by a redefinition of the basis states: $|m, A\rangle \rightarrow e^{i(m-1)(\phi_w + \phi_v)}|m, A\rangle$, and $|m, B\rangle \rightarrow e^{i\phi_v}e^{i(m-1)(\phi_v + \phi_w)}|m, B\rangle$.

More on this in an Exercise?

The matrix for the Hamiltonian of the SSH model, Eq. (1.1), represented in the a real-space basis $(|1, A\rangle, |1, B\rangle, |2, A\rangle, \dots)$, for a chain of $N = 4$ unit cells, reads

$$H = \begin{pmatrix} 0 & v & 0 & 0 & 0 & 0 & 0 & 0 \\ v & 0 & w & 0 & 0 & 0 & 0 & 0 \\ 0 & w & 0 & v & 0 & 0 & 0 & 0 \\ 0 & 0 & v & 0 & w & 0 & 0 & 0 \\ 0 & 0 & 0 & w & 0 & v & 0 & 0 \\ 0 & 0 & 0 & 0 & v & 0 & w & 0 \\ 0 & 0 & 0 & 0 & 0 & w & 0 & v \\ 0 & 0 & 0 & 0 & 0 & 0 & v & 0 \end{pmatrix}. \quad (1.2)$$

External and Internal Degrees of Freedom

There is a practical representation of this Hamiltonian, which emphasizes the separation of the external degrees of freedom (unit cell index m) from the internal degrees of freedom (sublattice index α). We can use a tensor product basis,

$$|m, \alpha\rangle \rightarrow |m\rangle \otimes |\alpha\rangle \in \mathcal{H}_{\text{external}} \otimes \mathcal{H}_{\text{internal}}, \quad (1.3)$$

with $m = 1, \dots, N$, and $\alpha \in \{A, B\}$. On this basis, with the Pauli matrices,

$$\sigma_0 = \begin{pmatrix} 1 & 0 \\ 0 & 1 \end{pmatrix}; \quad \sigma_x = \begin{pmatrix} 0 & 1 \\ 1 & 0 \end{pmatrix}; \quad \sigma_y = \begin{pmatrix} 0 & -i \\ i & 0 \end{pmatrix}; \quad \sigma_z = \begin{pmatrix} 1 & 0 \\ 0 & -1 \end{pmatrix}, \quad (1.4)$$

the Hamiltonian can be written as

$$\hat{H} = v \sum_{m=1}^N |m\rangle\langle m| \otimes \hat{\sigma}_x + w \sum_{m=1}^{N-1} \left(|m+1\rangle\langle m| \otimes \frac{\hat{\sigma}_x + i\hat{\sigma}_y}{2} + h.c. \right). \quad (1.5)$$

The intracell hopping shows up here as an onsite-potential-like intracell operator, while the intercell hopping as a hopping operator.

1.2 Bulk Hamiltonian

As every solid-state system, the long chain of the SSH model has a *bulk* and a *boundary*. The bulk is the long central part of the chain, the boundaries are the two ends, or “edges” of the chain, indicated by shading in Fig. 1.1. We first concentrate on the bulk, since, in the thermodynamic limit of $N \rightarrow \infty$, it is much larger than the boundaries, and it will determine the most important physical properties of the model. Although the treatment of the bulk using the Fourier transformation might seem like a routine step, we detail it here because different conventions are used in the literature. **(We might add more details at some point in a future Appendix.)**

The physics in the bulk, the long central part of the system, should not depend on how the edges are defined, and so for simplicity we set periodic (Born-von Karman) boundary conditions. This corresponds to closing the bulk part of the chain into a ring, with the bulk Hamiltonian defined as

$$\hat{H}_{\text{bulk}} = \sum_{m=1}^N (v|m, B\rangle \langle m, A| + w|(m \bmod N) + 1, A\rangle \langle m, B|) + h.c.. \quad (1.6)$$

We are looking for eigenstates of this Hamiltonian,

$$\hat{H}_{\text{bulk}} |\Psi_n(k)\rangle = E_n(k) |\Psi_n(k)\rangle, \quad (1.7)$$

with $n \in \{1, 2\}$, where k is the wavenumber and n is the band index, as explained below.

Bulk Momentum-Space Hamiltonian

Due to the translation invariance of the bulk, Bloch’s theorem applies, and we look for the eigenstates in a plane wave form. We introduce the plane wave basis states only for the external degree of freedom,

$$|k\rangle = \frac{1}{\sqrt{N}} \sum_{m=1}^N e^{imk} |m\rangle, \quad \text{for } k \in \{\delta_k, 2\delta_k, \dots, N\delta_k\} \quad \text{with } \delta_k = \frac{2\pi}{N}, \quad (1.8)$$

where the wavenumber k was chosen to take on values from the first Brillouin zone.

The *bulk momentum-space Hamiltonian* $\hat{H}(k)$ is defined using the plane-wave states,

$$\hat{H}(k) = \langle k | \hat{H}_{\text{bulk}} | k \rangle = \sum_{\alpha, \beta \in \{A, B\}} \langle k, \alpha | H_{\text{bulk}} | k, \beta \rangle \cdot |\alpha\rangle \langle \beta|. \quad (1.9)$$

Its eigenstates are vectors in the internal Hilbert space, $|u_n(k)\rangle \in \mathcal{H}_{\text{internal}}$,

$$\hat{H}(k) |u_n(k)\rangle = E_n(k) |u_n(k)\rangle; \quad |u_n(k)\rangle = a_n(k) |A\rangle + b_n(k) |B\rangle. \quad (1.10)$$

The Bloch states are eigenstates of the bulk Hamiltonian, and read

$$|\Psi_n(k)\rangle = |k\rangle \otimes |u_n(k)\rangle. \quad (1.11)$$

As an example, take the SSH model on a chain of $N = 4$ unit cells. Then, by inserting Eq. (1.11) into the Schrödinger equation (1.7), the latter translates to the following matrix eigenvalue equation:

$$\begin{pmatrix} 0 & v & 0 & 0 & 0 & 0 & 0 & w \\ v & 0 & w & 0 & 0 & 0 & 0 & 0 \\ 0 & w & 0 & v & 0 & 0 & 0 & 0 \\ 0 & 0 & v & 0 & w & 0 & 0 & 0 \\ 0 & 0 & 0 & w & 0 & v & 0 & 0 \\ 0 & 0 & 0 & 0 & v & 0 & w & 0 \\ 0 & 0 & 0 & 0 & 0 & w & 0 & v \\ w & 0 & 0 & 0 & 0 & 0 & v & 0 \end{pmatrix} \begin{pmatrix} a(k)e^{ik} \\ b(k)e^{ik} \\ a(k)e^{2ik} \\ b(k)e^{2ik} \\ a(k)e^{3ik} \\ b(k)e^{3ik} \\ a(k)e^{Nik} \\ b(k)e^{Nik} \end{pmatrix} = E(k) \begin{pmatrix} a(k)e^{ik} \\ b(k)e^{ik} \\ a(k)e^{2ik} \\ b(k)e^{2ik} \\ a(k)e^{3ik} \\ b(k)e^{3ik} \\ a(k)e^{Nik} \\ b(k)e^{Nik} \end{pmatrix}. \quad (1.12)$$

The Schrödinger equation defining the matrix $H(k)$ of the bulk momentum-space Hamiltonian reads

$$H(k) = \begin{pmatrix} 0 & v + we^{-ik} \\ v + we^{ik} & 0 \end{pmatrix}; \quad H(k) \begin{pmatrix} a(k) \\ b(k) \end{pmatrix} = E(k) \begin{pmatrix} a(k) \\ b(k) \end{pmatrix}. \quad (1.13)$$

Periodicity in Wavenumber

Although Eq. (1.11) has a lot to do with the continuous-variable Bloch theorem, $\Psi_{n,k}(x) = e^{ikx}u_{n,k}(x)$, this correspondence is not direct. In a discretization of the continuous-variable Bloch theorem, the internal degree of freedom would play the role of the coordinate within the unit cell, which is also transformed by the Fourier transform. Thus, the function $u_{n,k}(x)$ is periodic in real space, $u_{n,k}(x+1) = u_{n,k}(x)$, but not periodic in the Brillouin zone, $u_{n,k+2\pi}(x+1) \neq u_{n,k}(x)$. Our Fourier transform acts only on the external degree of freedom, and as a result, we have periodicity in the Brillouin zone,

$$\hat{H}(k+2\pi) = \hat{H}(k); \quad |\langle u_n(k) | u_n(k+2\pi) \rangle| = 1. \quad (1.14)$$

A condition for the latter is that the energy $E_n(k)$ is non-degenerate and therefore $|u_n(k)\rangle$ is well defined up to a global complex phase factor. This periodicity in Eq. (1.14) simplifies the formulas for the topological invariants immensely. Note, however, that the other convention, the discretization of the Bloch theorem, is also widely used in the literature. **We will compare the two approaches in a future Appendix.**

1.2.1 A Staggered Hopping Opens a Gap

The dispersion relation of the bulk can be read off from Eq. (1.13), using the fact that $\hat{H}(k)^2 = E(k)^2 \mathbb{1}_2$. This gives us

$$E(k) = \pm \left| v + e^{-ik}w \right| = \pm \sqrt{v^2 + w^2 + 2vw \cos k}. \quad (1.15)$$

We show this dispersion relation for five choices of the parameters in Figs. 1.2a-e.

As long as the hopping amplitudes are staggered, $v \neq w$, (Fig. 1.2a,b,d,e), there is an energy gap of 2Δ separating the lower, filled band, from the upper, empty band, with

$$\Delta = \min_k |E(k)| = |v - w|. \quad (1.16)$$

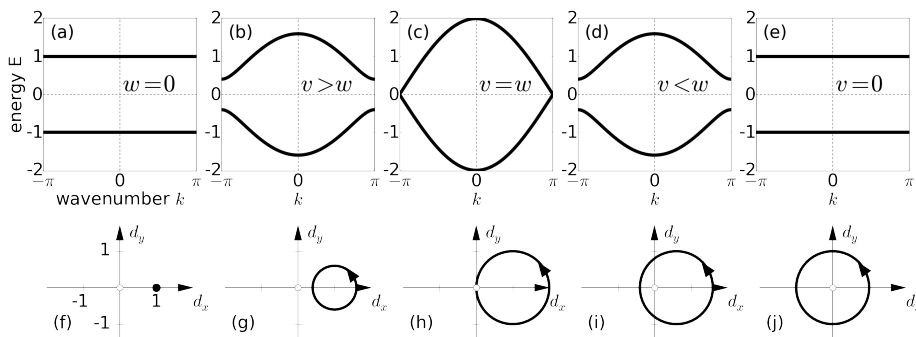


Figure 1.2: Dispersion relations of the SSH model, Eq. (1.15), for five settings of the hopping amplitudes: (a): $v = 1, w = 0$; (b): $v = 1, w = 0.6$; (c): $v = w = 1$; (d): $v = 0.6, w = 1$; (e): $v = 0, w = 1$. In each case, the path of the endpoints of the vector $\mathbf{d}(k)$ representing the bulk momentum-space Hamiltonian, Eqs. (1.17) and (1.18), are also shown on the d_x, d_y plane, as the wavenumber is swept across the Brillouin zone, $k = 0 \rightarrow 2\pi$; see (f)-(j).

Without the staggering, i.e., if $v = w$, (Fig. 1.2c), the SSH model describes a conductor. In that case there are plane wave eigenstates of the bulk available with arbitrarily small energy, which can transport electrons from one end of the chain to the other.

On an interesting note, we mention that the staggering of the hopping amplitudes occurs naturally in many solid state systems, e.g., polyacetylene, by what is known as the Peierls instability. A detailed analysis of this process necessitates a model where the positions of the atoms are also dynamical [32]. Nevertheless, we can understand this process intuitively just from the effects of a slight staggering on the dispersion relation. As the gap due to the staggering of the hopping amplitudes opens, the energy of occupied states is lowered, while unoccupied states move to higher energies. Thus, the staggering is energetically favourable.

1.2.2 Information Beyond the Dispersion Relation

Although the dispersion relation is useful to read off a number of physical properties of the bulk of the system (e.g., group velocities), there is also important information about the bulk that it does not reveal. Stationary states do not only have an energy and wavenumber eigenvalue, but also an internal structure, represented by the components of the corresponding vector $|u_n(k)\rangle \in \mathcal{H}_{\text{internal}}$. We now define a compact representation of this information for the SSH model.

The bulk momentum-space Hamiltonian $\hat{H}(k)$ of any two-band model (i.e., a model with 2 internal states per unit cell), reads

$$\hat{H}(k) = d_0(k)\hat{\sigma}_0 + d_x(k)\hat{\sigma}_x + d_y(k)\hat{\sigma}_y + d_z(k)\hat{\sigma}_z = d_0(k)\hat{\sigma}_0 + \mathbf{d}(k)\hat{\sigma}. \quad (1.17)$$

For the SSH model, see the Hamiltonian in Eq. (1.13), we have $d_0(k) = 0$, and the real

numbers $d_{x,y,z} \in \mathbb{R}$, the components of the k -dependent 3-dimensional vector $\mathbf{d}(k)$, read

$$d_x(k) = v + w \cos k; \quad d_y(k) = w \sin k; \quad d_z(k) = 0. \quad (1.18)$$

The internal structure of the eigenstates with momentum k is given by the direction in which the vector $\mathbf{d}(k)$ of Eq. (1.18) points (the energy is given by the magnitude of $\mathbf{d}(k)$; for details see Sect. 2.5).

As the wavenumber runs through the Brillouin zone, $k = 0 \rightarrow 2\pi$, the path that the endpoint of the vector $\mathbf{d}(k)$ traces out is a closed circle of radius w on the d_x, d_y plane, centered at $(v, 0)$. For more general 2-band insulators, this path need not be a circle, but it needs to be a closed loop due to the periodicity of the bulk momentum-space Hamiltonian, Eq. (1.14), and it needs to avoid the origin, to describe an insulator. If the loop is confined on the d_x, d_y plane, its topology can be characterized by an integer, the *bulk winding number* ν . This counts the number of times the loop winds around the origin of the d_x, d_y plane. For example, in Fig. 1.2f,g, we have $\nu = 0$, in Fig. 1.2i,j, we have $\nu = 1$, while in Fig. 1.2h, the winding number ν is undefined.

1.3 Edge States

Like any material, the SSH Hamiltonian does not only have a bulk part, but also boundaries (which we refer to as *ends* or *edges*). We can expect that in the bulk part, i.e., far away from the boundaries, local physical properties of the system are well approximated by calculations using periodic boundary conditions. Near the edges, though, local physical properties can be quite different. We can find, for example, that eigenstates of the Hamiltonian exist with energy in the gap of the bulk Hamiltonian: such states must be edge states, with wavefunctions that decrease exponentially towards the bulk. In case the bulk is translation invariant, bulk eigenstates will be extended but edge states localized in the thermodynamic limit of infinite system size. In this section we will begin with the so-called fully dimerized limits of the SSH model, where the edge regions can be unambiguously defined. We then move away from these limits, and use a practical definition of edge states.

1.3.1 Fully Dimerized Limits

The SSH model becomes particularly simple in the two fully dimerized cases: if the intercell hopping amplitude vanishes and the intracell hopping is set to 1, i.e., $\nu = 1, w = 0$, or vice versa, $\nu = 0, w = 1$. In both cases the SSH chain falls apart to a sequence of disconnected dimers, as shown in Fig. 1.3.

The Bulk in the Fully Dimerized Limits Has Flat Bands

In the fully dimerized limits, one can choose a set of energy eigenstates which are restricted to one dimer each. These consist of the even (energy $E = +1$) and odd (energy $E = -1$) superpositions of the two sites forming a dimer.

In the $\nu = 1, w = 0$ case, which we call *trivial*, we have

$$\nu = 1, w = 0: \quad \hat{H}(|m, A\rangle \pm |m, B\rangle) = \pm(|m, A\rangle \pm |m, B\rangle). \quad (1.19)$$

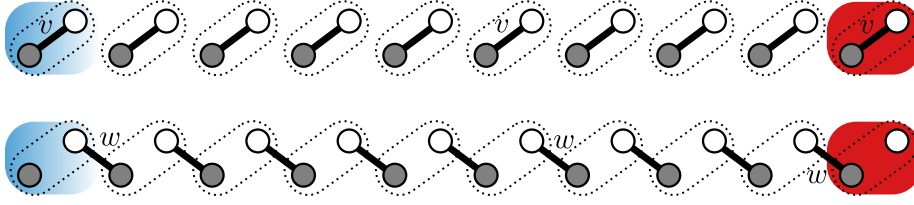


Figure 1.3: Fully dimerized limits of the SSH model, where the chain has fallen apart to disconnected dimers. In the trivial case (top, only intracell hopping, $v = 1, w = 0$), every energy eigenstate is an even or an odd superposition of single-site basis states in the same unit cell. In the topological case, (bottom, only intercell hopping, $v = 0, w = 1$), dimers are shared between neighboring unit cells. Then there is a single isolated site on each edge, that must host one eigenstate (per edge), at zero energy, since there are no onsite potentials.

The bulk momentum-space Hamiltonian is $\hat{H}(k) = \hat{\sigma}_x$, independent of the wavenumber k .

In the $v = 0, w = 1$ case, which we call *topological*, each dimer is shared between two neighboring unit cells,

$$v = 0, w = 1 : \quad \hat{H}(|m, B\rangle \pm |m+1, A\rangle) = \pm(|m, B\rangle \pm |m+1, A\rangle), \quad (1.20)$$

for $m = 1, \dots, N-1$. The bulk momentum-space Hamiltonian now is $\hat{H}(k) = \hat{\sigma}_x \cos k + \hat{\sigma}_y \sin k$.

In both fully dimerized limits, we can superpose the above-defined localized eigenstates to form Bloch-type energy eigenstates. These Bloch states inherit the same spectrum, $E(k) = \pm 1$, i.e., we have dispersionless or *flat bands* in this case, as seen in Fig. 1.2a and e. As a consequence, the group velocity is zero throughout each band – as the chain falls apart to dimers, a particle input into the bulk will not move along the chain.

The Edges in the Fully Dimerized Limit Can Host Zero Energy States

In the trivial case, $v = 1, w = 0$, all energy eigenstates of the SSH chain are given by the formulas of the bulk, Eq. (1.19). A topological, fully dimerized SSH chain, with $v = 0, w = 1$, however, has more energy eigenstates than those listed Eq. (1.20). Each end of the chain hosts a single eigenstate at zero energy,

$$v = 0, w = 1 : \quad \hat{H}|1, A\rangle = \hat{H}|N, B\rangle = 0. \quad (1.21)$$

These eigenstates have support on one site only. Their energy is zero because onsite potentials are not allowed in the SSH model. These are the simplest examples of *edge states*.

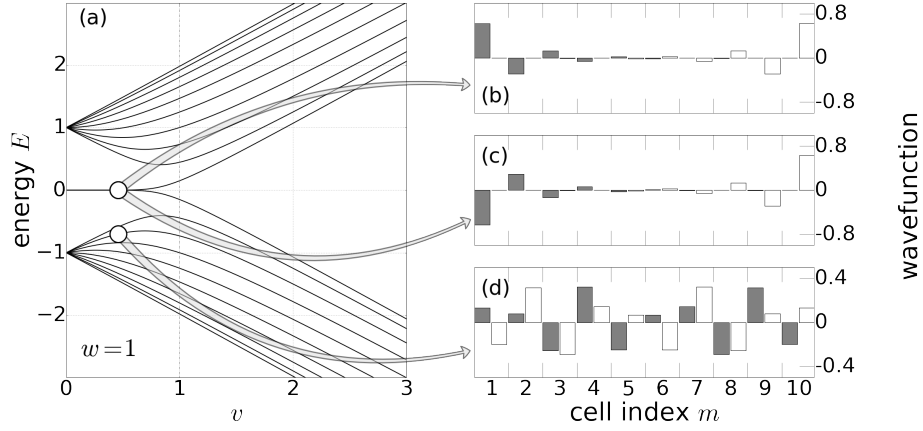


Figure 1.4: Energy spectrum and wave functions of a finite-sized SSH model. The number of unit cells is $N = 10$. (a) Energy spectrum of the system for intercell hopping amplitude $w = 1$ as a function of the intracell hopping amplitude v . $v < 1$ ($v > 1$) corresponds to the topological (trivial) phases. (b) and (c) show the wave functions of the hybridized edge states, while (d) shows a generic bulk wave function.

1.3.2 Moving Away from the Fully Dimerized Limit

We now examine what happens to the edge states as we move away from the fully dimerized limit. To be specific, we examine how the spectrum of an open topological chain, $v = 0, w = 1$, of $N = 10$ unit cells changes, as we continuously turn on the intracell hopping amplitude v . The spectra, Fig. 1.4a, reveal that the energies of the edge states remain very close to zero energy.

The wavefunctions of almost-zero-energy edge states have to be exponentially localized at the left/right edge, because the zero of energy is in the bulk band gap. A plot of the wavefunctions (which have only real components, since the Hamiltonian is real), Figs. 1.4b and c, reveal that the almost-zero-energy eigenstates are odd and even superpositions of states localized exponentially on the left and the right edge. This is a result of the exponentially small overlap between the left and the right edge states. We will later show, in Sect. 1.5.2, that the edge-state energies are also controlled by this overlap, and are of the order $E = e^{-N/\xi}$, with a localization length $\xi = 1/\log(v/w)$.

There is an important property of the edge states, which is only revealed by the plot of their wavefunctions, Fig. 1.4b and c. The right edge state has nonvanishing components only on the A sublattice while the left edge state is on the B sublattice.

In the following, we show the generality of these properties, and show the link between the bulk winding number and the presence/absence of edge states, known as bulk–boundary correspondence. In the case of the SSH model, all this hinges on a property of the model known as chiral symmetry.

1.4 Chiral Symmetry

The SSH model has a very important property, that is often referred to as chiral (or sublattice) symmetry. It is the property that all nonvanishing matrix elements of the Hamiltonian connect sites on different sublattices. We here discuss unitary symmetries, define chiral symmetry, and flesh out its consequences.

Unitary Symmetries are Eliminated

In quantum mechanics, we say that a Hamiltonian \hat{H} has a symmetry represented by a unitary operator \hat{U} if

$$\hat{U}\hat{H}\hat{U}^\dagger = \hat{H}. \quad (1.22)$$

In case of a symmetry, \hat{U} and \hat{H} can be diagonalized together, and therefore, \hat{H} has no matrix elements between two eigenstates of \hat{U} with different eigenvalues. This can be understood as a superselection rule: if we partition the Hilbert space into different sectors, i.e., eigenspaces of \hat{U} , labeled by the corresponding eigenvalues, then the dynamics as defined by \hat{H} can be regarded separately in each sector.

A unitary symmetry can be simply made to disappear if we restrict ourselves to one sector of the Hilbert space. This is what we do anyway if we want to diagonalize the Hamiltonian efficiently, and we know that it has a given unitary symmetry. An extreme example is that of lattice translation symmetry. In Sect. 1.2, to simplify the bulk Hamiltonian, we essentially rewrote it in the basis of plane wave modes. In this basis it became block diagonal, with its 2x2 blocks given by the bulk momentum-space Hamiltonian, evaluated at the one wavenumber per block. There the symmetry was the lattice translation operator $\hat{U} = |(m \bmod N) + 1, A\rangle \langle m, A| + |m + 1, B\rangle \langle m, B|$, and the labels of the superselection sectors were the quasimomenta k . The 2x2 blocks of \hat{H} , obviously had no translation symmetry left.

A Different Type of Symmetry

The word ‘‘symmetry’’ is also used in a different sense in condensed matter physics. One example is chiral symmetry. We say that a system with Hamiltonian \hat{H} has *chiral symmetry*, if

$$\hat{\Gamma}\hat{H}\hat{\Gamma}^\dagger = -\hat{H}, \quad (1.23)$$

with an operator $\hat{\Gamma}$ that is not only unitary, but fulfils some other criteria as well. Notice the extra minus sign on the right hand side. This has important consequences, which we come to later, but first discuss the criteria on the symmetry operator.

First, in order to exclude conventional unitary symmetries (we assume those have already been eliminated), the chiral symmetry operator has to be not only unitary but Hermitian as well, $\hat{\Gamma}^\dagger = \hat{\Gamma}$. This can be written succinctly as

$$\hat{\Gamma}^\dagger \hat{\Gamma} = \hat{\Gamma}^2 = 1. \quad (1.24)$$

To understand where the requirement of hermiticity comes from, consider the operator $\hat{\Gamma}^2$. This represents a conventional unitary symmetry of \hat{H} , since

$$\hat{\Gamma}^2 \hat{H} (\hat{\Gamma}^2)^\dagger = \hat{\Gamma} (\hat{\Gamma} \hat{H} \hat{\Gamma}^\dagger) \hat{\Gamma}^\dagger = -\hat{\Gamma} \hat{H} \hat{\Gamma}^\dagger = \hat{H}. \quad (1.25)$$

In order not to have unitary symmetries, we require that the square of the chiral symmetry operator is a (state-independent) phase, $\hat{\Gamma}^2 = e^{i\phi}$. Requiring $\hat{\Gamma}^2 = 1$ is no loss of generality, because we can always “gauge the phase away” by $\hat{\Gamma} \rightarrow e^{-i\phi/2} \hat{\Gamma}$.

Second, it is also required that the sublattice operator $\hat{\Gamma}$ be local. The system is assumed to consist of unit cells, and matrix elements of $\hat{\Gamma}$ between sites from different unit cells should vanish. In the SSH chain, this means that for $m \neq m'$, we have $\langle m, \alpha | \hat{\Gamma} | m', \alpha' \rangle = 0$, for any $\alpha, \alpha' \in (A, B)$. To keep things simple, we can demand that the sublattice operator act in the same way in each unit cell (although this is not strictly necessary), its action represented by a unitary operator $\hat{\gamma}$ acting on the internal Hilbert space of one unit cell, i.e.,

$$\hat{\Gamma} = \hat{\gamma} \oplus \hat{\gamma} \oplus \dots \oplus \hat{\gamma} = \bigoplus_{m=1}^N \hat{\gamma}, \quad (1.26)$$

where N is the number of unit cells.

A third requirement, which is often not explicitly stated, is that the chiral symmetry has to be *robust*. To understand what we mean by that, first note that in solid state physics, we often deal with Hamiltonians with many local parameters that vary in a controlled or uncontrolled way. An example is the SSH model, where the values of the hopping amplitudes could be subject to spatial disorder. We gather all such parameters in a formal vector, and call it $\underline{\xi} \in \Xi$. Here Ξ is the set of all realizations of disorder that we investigate. Instead of talking about the symmetries of a Hamiltonian \hat{H} , we should rather refer to symmetries of a set of Hamiltonians $\{\hat{H}(\underline{\xi})\}$, for all $\underline{\xi} \in \Xi$. This set has chiral symmetry represented by $\hat{\Gamma}$ if

$$\forall \underline{\xi} \in \Xi: \quad \hat{\Gamma} \hat{H}(\underline{\xi}) \hat{\Gamma} = -\hat{H}, \quad (1.27)$$

with the symmetry operator $\hat{\Gamma}$ independent of the parameters $\underline{\xi}$. This is the robustness of the chiral symmetry.

Sublattice Symmetry

Chiral symmetry is also called *sublattice symmetry*. Given the chiral symmetry operator $\hat{\Gamma}$, we can define orthogonal sublattice projectors \hat{P}_A and \hat{P}_B , as

$$\hat{P}_A = \frac{1}{2} (\mathbb{I} + \hat{\Gamma}); \quad \hat{P}_B = \frac{1}{2} (\mathbb{I} - \hat{\Gamma}), \quad (1.28)$$

where \mathbb{I} represents the identity operator on the Hilbert space of the system. Note that $\hat{P}_A + \hat{P}_B = \mathbb{I}$, and $\hat{P}_A \hat{P}_B = 0$. The defining relation of sublattice symmetry, Eq. (1.23), can be written in an equivalent form by requiring that the Hamiltonian induces no transitions from any site on one sublattice to any site on the same sublattice,

$$\hat{P}_A \hat{H} \hat{P}_A = \hat{P}_B \hat{H} \hat{P}_B = 0; \quad \hat{H} = \hat{P}_A \hat{H} \hat{P}_B + \hat{P}_B \hat{H} \hat{P}_A. \quad (1.29)$$

In fact, using the projectors \hat{P}_A and \hat{P}_B is an alternative and equivalent way of defining chiral symmetry. The operator representing the symmetry is then $\hat{\Gamma} = \hat{P}_A - \hat{P}_B$.

Block Off-diagonal structure in the chiral basis

In general, chiral symmetry guarantees that the matrix of the Hamiltonian is block off-diagonal in a practically chosen basis, a chiral basis. This is similar to how unitary symmetry guarantees a block diagonal structure in a basis that takes into account the corresponding symmetry. A chiral basis is such that every basis state is an eigenstate of the chiral symmetry, and they are ordered so that all the states with eigenvalue $+1$ (sublattice A) come first, and then all the states with eigenvalue -1 follow. In other words, in the chiral basis,

$$\text{chiral basis: } \hat{\Gamma} = \text{diag}(\underbrace{1, \dots, 1}_{N_A}, \underbrace{-1, \dots, -1}_{N_B}), \quad (1.30)$$

where, for the SSH model, $N_A = N_B = N$. Chiral symmetry is tantamount to requiring that the matrix of the Hamiltonian, in the chiral basis, should be block *off-diagonal*,

$$\hat{H} = \begin{pmatrix} 0 & h \\ h^\dagger & 0 \end{pmatrix}, \quad (1.31)$$

where h is an $N_A \times N_B$ matrix.

d

1.4.1 Consequences of Chiral Symmetry for Energy Eigenstates

We now come to the consequences of chiral symmetry, which are very different from those of conventional symmetries, due to the extra minus sign in its definition, Eq. (1.23).

Symmetric Spectrum

The spectrum of a chiral symmetric Hamiltonian is symmetric with respect to the $E = 0$ line. For any state with energy E , there is a chiral symmetric partner with energy $-E$. This is simply seen,

$$\hat{H}|\psi\rangle = E|\psi\rangle \implies \hat{H}\hat{\Gamma}|\psi\rangle = -\hat{\Gamma}\hat{H}|\psi\rangle = -\hat{\Gamma}E|\psi\rangle = -E\hat{\Gamma}|\psi\rangle. \quad (1.32)$$

This carries different implications for nonzero energy eigenstates and zero energy eigenstates.

For $E \neq 0$, the states $|\psi\rangle$ and $\hat{\Gamma}|\psi\rangle$ are eigenstates with different energy, and, therefore, have to be orthogonal. This implies that every nonzero energy eigenstate of \hat{H} has equal support on both sublattices,

$$\text{If } E \neq 0: \quad \langle \psi | \hat{P}_A | \psi \rangle = \langle \psi | \hat{P}_B | \psi \rangle, \quad (1.33)$$

which follows from $\langle \psi | \hat{\Gamma} | \psi \rangle = 0$.

For $E = 0$, zero energy eigenstates can be chosen to have support on only one sublattice, i.e.,

$$\text{If } E = 0: \quad \hat{H}\hat{P}_{A/B}|\psi\rangle = \frac{1}{2}\hat{H}(|\psi\rangle \pm \hat{\Gamma}|\psi\rangle) = 0. \quad (1.34)$$

These projected zero-energy eigenstates are eigenstates of $\hat{\Gamma}$, and therefore are chiral symmetric partners of *themselves*.

Just as unitary symmetries help obtain the spectrum of a Hamiltonian (diagonalization of the blocks is numerically cheaper than diagonalizing the whole matrix), so does chiral symmetry. We need to only calculate with the off-diagonal block of the Hamiltonian in the chiral basis, i.e., h of Eq. (1.31). This h is an $N_A \times N_B$ matrix, not necessarily a square matrix; we will take without loss of generality $N_A \leq N_B$. The eigenvalues and eigenvectors of H can be obtained from the singular value decomposition of h , i.e., from the spectrum of hh^\dagger . For every strictly positive eigenvalue E^2 of hh^\dagger , with eigenvector \mathbf{u} , there is a pair of eigenvectors of H , since

$$hh^\dagger \mathbf{u} = E^2 \mathbf{u} \quad \implies \quad \begin{pmatrix} 0 & h \\ h^\dagger & 0 \end{pmatrix} \begin{pmatrix} \pm E \mathbf{u} \\ h^\dagger \mathbf{u} \end{pmatrix} = \pm E \begin{pmatrix} \pm E \mathbf{u} \\ h^\dagger \mathbf{u} \end{pmatrix}. \quad (1.35)$$

Remark: Every zero eigenvalue of hh^\dagger gives a single zero-energy eigenstate of \hat{H} , that lives on sublattice A , obtained from the eigenvector \mathbf{u} of hh^\dagger as $(\mathbf{u}, 0)$ in a chiral basis. Similarly, zero eigenvalues of hh^\dagger can be used to construct zero-energy eigenstates of \hat{H} that live on sublattice B . If $N_A < N_B$, then we know hh^\dagger must have $N_B - N_A$ eigenvectors with eigenvalue 0. In other words, if there are more sites on one sublattice than on the other, the majority sublattice will host eigenstates that are exactly at zero energy.

1.4.2 Sublattice Projectors and Chiral Symmetry of the SSH Model

The Hamiltonian of the SSH model, Eq. (1.1), is *bipartite*: the Hamiltonian includes no transitions between sites with the same sublattice index. The projectors to the sublattices read

$$\hat{P}_A = \sum_{m=1}^N |m, A\rangle \langle m, A|; \quad \hat{P}_B = \sum_{m=1}^N |m, B\rangle \langle m, B|. \quad (1.36)$$

Chiral symmetry is represented by the sublattice operator $\hat{\Sigma}_z$, that multiplies all components of a wavefunction on sublattice B by (-1) ,

$$\hat{\Sigma}_z = \hat{P}_A - \hat{P}_B. \quad (1.37)$$

Note that this operator has the properties required of the chiral symmetry operator above: it is unitary, Hermitian, and local.

The chiral symmetry of the SSH model is a restatement of the fact that the Hamiltonian is bipartite,

$$\hat{P}_A \hat{H} \hat{P}_A = \hat{P}_B \hat{H} \hat{P}_B = 0; \quad \Leftrightarrow \quad \hat{\Sigma}_z \hat{H} \hat{\Sigma}_z = -\hat{H}. \quad (1.38)$$

This relation holds because \hat{H} only contains terms that are multiples of $|m, A\rangle \langle m', B|$, or of $|m, B\rangle \langle m', A|$ with $m, m' \in \mathbb{Z}$. Upon multiplication from the left and the right by $\hat{\Sigma}_z$, such a term picks up a single factor of -1 (because of the multiplication from the left or because of the multiplication from the right). Note that this relation, equivalent to an anticommutation of \hat{H} and $\hat{\Sigma}_z$, holds whether or not the hopping amplitudes depend on position: therefore, the chiral symmetry represented by $\hat{\Sigma}_z$ has the required property of robustness.

1.4.3 Consequence of Chiral Symmetry: Bulk Winding Number ν for the SSH Model

We now consider the bulk momentum-space Hamiltonian $\hat{H}(k) = \mathbf{d}(k) \hat{\sigma}$.

The path of the endpoint of $\mathbf{d}(k)$, as the wavenumber goes through the Brillouin zone, $k = 0 \rightarrow 2\pi$, is a closed path on the d_x, d_y plane. This path has to avoid the origin, $\mathbf{d} = 0$: if there was a k at which $\mathbf{d}(k) = 0$, the gap would close at this k , and we would not be talking about an insulator. Because of chiral symmetry, the vector $\mathbf{d}(k)$ is restricted to lie on the d_x, d_y plane,

$$\hat{\sigma}_z \hat{H}(k) \hat{\sigma}_z = -\hat{H}(k) \quad \implies \quad d_z(k) = 0. \quad (1.39)$$

The endpoint of $\mathbf{d}(k)$ is then a closed, directed loop on the plane, and thus has a well defined integer *winding number* about the origin.

Winding Number ν as the Multiplicity of Solutions

A simple way to obtain the winding number graphically is counting the number of times $\mathbf{d}(k)$ intersects a curve that goes from the origin of the d_x, d_y plane to infinity.

1. Since $\mathbf{d}(k)$ is a directed curve, it has a left side and a right side. Paint the left side blue, the right side red, as shown in Fig. 1.5a.

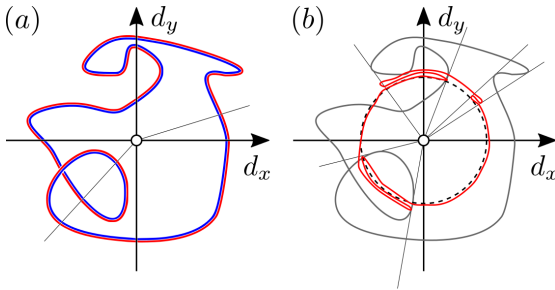


Figure 1.5: (a) Endpoints of the vector $\mathbf{d}(k)$ forming a loop, as k is swept through the Brillouin zone. Red/blue denotes the left/right side of the loop. (b) The loop (gray) is projected to the unit circle (dashed). This projection (red) allows for the compact formula (1.41) expressing the winding number of the loop around the origin. **We should display a few arrows showing the direction of the directed curves, both on (a) and (b).**

2. Take a directed curve \mathcal{L} going from 0 to infinity. We can call this the “line of sight to infinity”, although it need not be a straight line. A simple choice is the half-infinite line, $d_y = 0$, $d_x \geq 0$. Two other choices are shown in Fig. 1.5a.
3. Identify the intersections of $\mathbf{d}(k)$ with \mathcal{L} .
4. Each intersection has a signature: this is $+1$ if the line of sight meets it from the blue side, -1 for the red side.
5. The winding number ν is the sum of the signatures.

We now consider how the winding number ν defined above can change under continuous deformations of \mathcal{L} or of $\mathbf{d}(k)$. We only allow for deformations that keep both curves on the plane, maintain \mathcal{L} going from the origin to infinity, and do not create points where $\mathbf{d}(k) = 0$. Due to the deformations the intersections of \mathcal{L} and $\mathbf{d}(k)$ can move, but this does not change ν . They can also appear or disappear, at points where \mathcal{L} and $\mathbf{d}(k)$ touch. However, they can only appear or disappear pairwise: a red and a blue intersection together, which does not change ν . As an example, the two choices of the line of sight \mathcal{L} in Fig. 1.5a, have 1 or 3 intersections, but the winding number is $+1$, for either of them.

Winding Number as an Integral

The winding number can also be written as a compact formula using the unit vector $\tilde{\mathbf{d}}$, defined as

$$\tilde{\mathbf{d}} = \frac{\mathbf{d}}{|\mathbf{d}|}. \quad (1.40)$$

The image of the map $\tilde{\mathbf{d}}$ is the red loop shown in Fig. 1.5b: it is the projection of the curve of $\mathbf{d}(k)$ (gray loop) to the unit circle (dashed). The vector $\tilde{\mathbf{d}}(k)$ is well defined for all k because $\mathbf{d}(k) \neq 0$. You can check easily that the winding number ν is given by

$$\nu = \frac{1}{2\pi} \int \left(\tilde{\mathbf{d}}(k) \times \frac{d}{dk} \tilde{\mathbf{d}}(k) \right)_z dk. \quad (1.41)$$

To calculate ν directly from the bulk momentum-space Hamiltonian, note that it is off-diagonal (in the basis of eigenstates of the chiral symmetry operator $\hat{\sigma}_z$),

$$H(k) = \begin{pmatrix} 0 & h(k) \\ h^*(k) & 0 \end{pmatrix}; \quad h(k) = d_x(k) - id_y(k). \quad (1.42)$$

The winding number of $\mathbf{d}(k)$ can be written as an integral, using the complex logarithm function, $\log(|h|e^{i\arg h}) = \log|h| + i\arg h$. It is easy to check that

$$\nu = \frac{1}{2\pi i} \int_{-\pi}^{\pi} dk \frac{d}{dk} \log h(k) = \frac{1}{2\pi i} \lim_{M \rightarrow \infty} \sum_{j=1}^{M-1} \log \frac{h(k=2\pi(j+1)/M)}{h(k=2\pi j/M)}. \quad (1.43)$$

Here, during the calculation of the integral, the branch cut for the logarithm is always shifted so that the derivative is always well defined. The above integral is always imaginary, and thus, ν is always real, since $|h(k=-\pi)| = |h(k=\pi)|$.

Winding Number of the SSH Model

For the SSH model, the winding number is either 0 or 1, depending on the parameters. In the trivial case, when the intracell hopping dominates the intercell hopping, $v > w$, the winding number is $\nu = 0$. In the topological case, when $w > v$, we have $\nu = 1$.

To change the winding number ν of the SSH model, we need to either (a) pull the path of $\mathbf{d}(k)$ through the origin in the d_x, d_y plane, or (b) lift it out of the plane and put it back on the plane at a different position. This is illustrated in Fig. 1.6. Method (a) requires closing the bulk gap. Method (b) requires breaking chiral symmetry.

1.5 Number of Edge States as Topological Invariant

We now introduce the notion of *adiabatic deformation* of insulating Hamiltonians. An insulating Hamiltonian is adiabatically deformed if

- its parameters are changed continuously,
- but the important symmetries of the system are always maintained,
- and the bulk gap around $E = 0$ remains open.

The deformation is a fictitious process, and does not take place in time. However, if we do think of it as a process in real time, the adiabatic theorem [15] tells us, that,

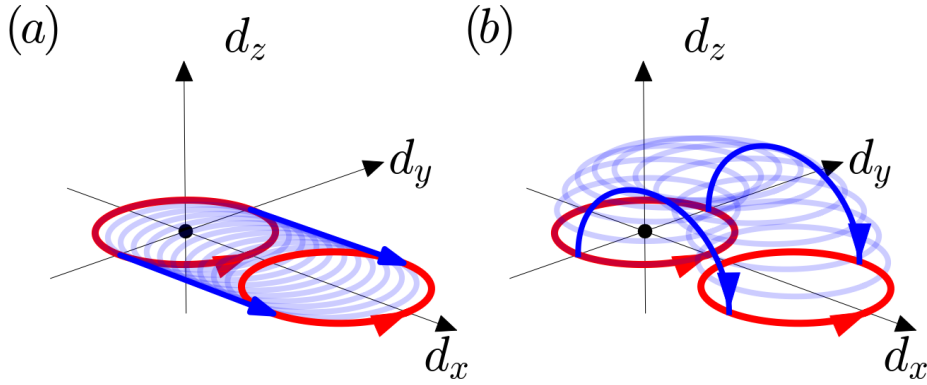


Figure 1.6: The endpoints of the vector $\mathbf{d}(k)$ as k goes across the Brillouin zone (red or blue closed circles), for various parameter settings in the SSH model. In (a), intercell hopping is kept constant at $w = 1$, while the intracell hopping is increased from $v = 0$ to $v = 2.3$. In the process, the bulk gap was closed and reopened, as the origin (black point) falls on one of the blue circles. The winding number is changed from 1 to 0. In (b), we again keep $w = 1$, and increase v from 0 to 2.3, but this time avoid closing the bulk gap by introducing a sublattice potential, $H_{\text{sublattice}} = u\hat{\sigma}_z$. We do this by tuning a parameter θ from 0 to π , and setting $v = 1.15(1 - \cos \theta)$, and $u = \sin \theta$. At the end of the process, $\theta = \pi$, there is no sublattice potential, so chiral symmetry is restored. The winding number has been changed from 1 to 0.

starting from the many-body ground state (separated from excited states by the energy gap), and performing the deformation slowly enough, we end up in the ground state, at least as far as the bulk of the system is concerned. Note that for any finite system with edges, changes can occur in the ground state even during an adiabatic deformation (with a subtle point to be made about how the adiabatic deformations has to be slow, but not too slow, that the edges can still be considered separately). We will come back to this point in Chap. 4.

Adiabatic Equivalence of Hamiltonians

Two insulating Hamiltonians are said to be *adiabatically equivalent* or *adiabatically connected* if there is an adiabatic deformation connecting them, that respects the important symmetries. For example, in the phase diagram Fig. 1.7 of the SSH model, the two Hamiltonians corresponding to the two black points in the topological phase ($w > v$) are adiabatically connected, as one can draw a path between them which does not cross the gapless topological-trivial phase boundary $w = v$.

Topological Invariant

We call an integer number characterizing an insulating Hamiltonian a *topological invariant*, or adiabatic invariant, if it cannot change under adiabatic deformations. Note that the use of adiabatic deformations implies two properties of the topological invariant: (1) it is only well defined in the thermodynamic limit, (2) it depends on the

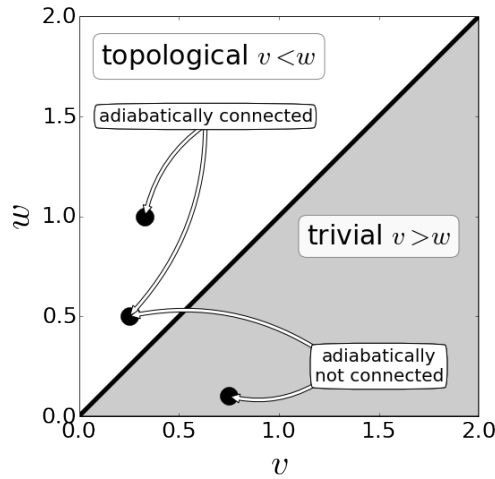


Figure 1.7: Phase diagram of the SSH model. The winding number of the bulk momentum-space Hamiltonian $\hat{H}(k)$ can be $\nu = 0$, if $\nu > w$, or $\nu = 1$, if $\nu < w$. This defines the trivial (gray) and the topological phase (white). The boundary separating these phases (black solid line), corresponds to $\nu = w$, where the bulk gap closes at some k . Two Hamiltonians in the same phase are adiabatically connected.

symmetries that need to be respected. An example for a topological invariant is the winding number ν of the SSH model.

We know that two insulating Hamiltonians are not adiabatically equivalent if their topological invariants differ. Consider as an example two Hamiltonians corresponding to two points on different sides of the phase boundary in Fig. 1.7 of the SSH model. They are not adiabatically connected in the phase diagram. Nevertheless, one might think that continuously modifying the bulk Hamiltonian by the addition of extra terms, while maintaining chiral symmetry, could lead to a connection between them. However, their winding numbers differ, and since winding numbers cannot change under adiabatic deformation, we know that they are not adiabatically equivalent.

Net Number of Edge States as a Topological Invariant

We have seen in Sect. 1.3.2, that the number of edge states at one end of the SSH model was an integer that did not change under a specific type of adiabatic deformation. We now generalize this example.

Consider energy eigenstates at the left end of a gapped chiral symmetric one-dimensional Hamiltonian in the thermodynamic limit, i.e., with length $N \rightarrow \infty$, in an energy window from $-\varepsilon < E < \varepsilon$, with ε in the bulk gap. There can be nonzero-energy edge states in this energy window, and zero-energy edge states as well. Each nonzero-energy state has to have a chiral symmetric partner, with the state and its partner occupying the same unit cells (the chiral symmetry operator is a local unitary). The number of zero-energy states is finite (because of the gap in the bulk), and they can be restricted to a single sublattice each. There are N_A zero-energy states at the left end on sublattice A , and N_B states on sublattice B . We can say that the *net* number of zero-energy states on the left end is $N_A - N_B$.

Consider the effect of an adiabatic deformation of the Hamiltonian, indexed by some continuous parameter $f : 0 \rightarrow 1$, on the net number of zero-energy edge states at the left end, $N_A - N_B$. The Hamiltonian respects chiral symmetry, and its bulk energy gap exceeds 2ε , for all values of f .

The deformation can create zero-energy states by bringing a nonzero-energy edge state $|\Psi_0(f=0)\rangle$ to zero energy, $E_0(f) = 0$ for $f \geq f'$ but not for $f < f'$. In that case, the chiral symmetric partner of $|\Psi_0\rangle$, which (up to a phase factor) is $\hat{\Gamma}|\Psi_0(f)\rangle$, has to move simultaneously to zero energy. The newly created zero energy edge states are $\hat{P}_A|\Psi_0(f')\rangle$ and $\hat{P}_B|\Psi_0(f')\rangle$, which occupy sublattice A and B , respectively. Thus, the net number $N_A - N_B$ is unchanged.

The deformation can also bring a zero energy state $|\Psi_0\rangle$ to energy $E > 0$ at some $f = f'$. However, it must also create a chiral symmetric partner with energy $E < 0$ at the same f' . This is the time reverse of the process of the previous paragraph: here, both N_A and N_B must decrease by 1, and, again, $N_A - N_B$ is unchanged.

The deformation can move nonzero-energy states in or out of the $-\varepsilon < E < \varepsilon$ energy window. This obviously has no effect on the number $N_A - N_B$.

Due to the deformation, the wavefunction of a zero-energy eigenstate can change so that it extends deeper and deeper into the bulk. However, because of the gap condition, zero-energy states have to have wavefunctions that decay exponentially towards the

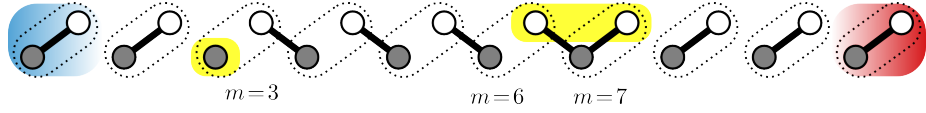


Figure 1.8: A long, fully dimerized SSH chain with 3 domains. The boundaries between the domains, the “domain walls”, host zero energy eigenstates (yellow shading). These can be localized on a single site, as for the domain wall at $m = 3$, or on a superposition of sites, as the odd superposition of the ends of the trimer shared between the $m = 6$ and $m = 7$ unit cells. .

bulk, and so this process cannot move them away from the edge. Thus, N_A and N_B cannot be changed this way.

The arguments above show that $N_A - N_B$, the net number of edge states on sublattice A at the left edge, is a topological invariant.

Bulk–Boundary Correspondence in the SSH Model

We have introduced two topological invariants for the SSH model: the winding number ν , of Eq. (1.41), and the net number of edge states at the left edge, $N_A - N_B$, in this section. The first one was obtained from the bulk Hamiltonian only, the second by looking at the low energy sector of the left edge. In the trivial case of the SSH model, $\nu > w$, both are 0; in the topological case, $\nu < w$, both are 1. This shows that we can use the bulk topological invariant (the winding number) to make simple robust predictions about the low-energy physics at the edge. This is a simple example for the *bulk–boundary correspondence*, a recurrent theme in the theory of topological insulators, which will reappear in various models in the forthcoming chapters.

1.5.1 Bound States at Domain Walls

Edge states do not only occur at the ends of an open chain, but also at domain walls between different insulating domains of the same chain. This can be understood via the fully dimerized limit. The example in Fig. 1.8 hosts two types of domain walls: one containing a single isolated site, which hosts a zero-energy state (no onsite potentials are allowed), and one containing a trimer. On a trimer, the odd superposition of the two end sites form a zero-energy eigenstate. In the example of Fig. 1.8, this is

$$\hat{H}(|6, B\rangle - |7, B\rangle) = 0. \quad (1.44)$$

Note that, just as the edge states at the ends of the chain, these zero-energy states at the domain walls have wavefunctions that take nonzero values on one sublattice only.

From a perfect dimerized phase without domains, it is only possible to germinate an even number of domain walls. This means that if one encounters a domain wall with a localized state on one sublattice then there will be another domain wall somewhere in the system—possibly at the system’s edge—with a localized state on the opposite sublattice.

Consider a domain wall in an SSH system that is not in the fully dimerized limit. The wavefunctions of the edge states at the domain walls will penetrate to some small depth into the bulk, with exponentially decaying evanescent tails. For two domain walls at a distance of M unit cells, the two edge states on the walls will hybridize, form “bonding” and “anti-bonding” states. At half filling, of these only the negative energy eigenstate will be occupied. This state hosts a single electron, however, its wavefunction is localized with equal weight on the two domain walls. Hence each domain wall, when well separated from other domain walls and the ends of the chain, will carry half an electronic charge. This effect is sometimes referred to as “fractionalization” of the charge.

1.5.2 Exact Calculation of Edge States

The zero energy edge states of the SSH model can also be calculated exactly, even in the absence of translational invariance. Take an SSH model on N unit cells, with complex intracell and intercell hopping amplitudes,

$$\hat{H} = \sum_{m=1}^N (v_m |m, B\rangle \langle m, A| + h.c.) + \sum_{m=1}^{N-1} (w_m |m+1, A\rangle \langle m, B| + h.c.). \quad (1.45)$$

We are looking for a zero energy eigenstate of this Hamiltonian,

$$\hat{H} \sum_{m=1}^N (a_m |m, A\rangle + b_m |m, B\rangle) = 0. \quad (1.46)$$

This gives us $2N$ linear homogeneous equations for the $2N$ amplitudes a_m and b_m , which read

$$m = 1, \dots, N-1: \quad v_m a_m + w_m^* a_{m+1} = 0; \quad w_m b_m + v_{m+1}^* b_{m+1} = 0; \quad (1.47a)$$

$$\text{boundaries:} \quad v_N a_N = 0; \quad v_1^* b_1 = 0. \quad (1.47b)$$

The first set of equations is solved by

$$m = 2, \dots, N: \quad a_m = \prod_{j=1}^{m-1} \frac{-v_j}{w_j^*} a_1; \quad (1.48)$$

$$m = 1, \dots, N-1: \quad b_m = \frac{-v_N}{w_m} \prod_{j=m+1}^{N-1} \frac{-v_j^*}{w_j} b_N. \quad (1.49)$$

However, we also have to fulfil Eq. (1.47b), which give

$$b_1 = a_N = 0. \quad (1.50)$$

These equations together say that, in the generic case, there is no zero energy eigenstate, $a_m = b_m = 0$.

Although there is no exactly zero energy state, Eqs. (1.48), (1.49) and (1.50) admit two approximate solutions in the thermodynamic limit, $N \rightarrow \infty$, if the average intercell

hopping is stronger than the intracell hopping. More precisely, we define the “bulk average values”,

$$\overline{\log|v|} = \frac{1}{N-1} \sum_{m=1}^{N-1} \log|v_m|; \quad \overline{\log|w|} = \frac{1}{N-2} \sum_{m=2}^{N-1} \log|w_m|. \quad (1.51)$$

Equations (1.48) and (1.49) translate to

$$|a_N| = |a_1| e^{-(N-1)/\xi}; \quad |b_1| = |b_N| e^{-(N-2)/\xi} \frac{|v_N|}{|v_1|}, \quad (1.52)$$

with the localization length

$$\xi = \frac{1}{\overline{\log|w|} - \overline{\log|v|}}. \quad (1.53)$$

If in the thermodynamic limit, the bulk average values, Eq. (1.51) make sense, and $\xi > 0$, we have two approximate zero energy solutions,

$$|L\rangle = \sum_{m=1}^N a_m |m, A\rangle; \quad |R\rangle = \sum_{m=1}^N b_m |m, B\rangle, \quad (1.54)$$

with the coefficients a_m and b_m chosen according to Eqs. (1.48) and (1.49), and a_1 , respectively, b_N , used to fix the norm of $|L\rangle$, respectively, $|R\rangle$.

Hybridization of Edge States

The two states $|L\rangle$ and $|R\rangle$ hybridize under \hat{H} to an exponentially small amount, and this induces a small energy splitting. We can obtain an estimate for the splitting, and the energy eigenstates, to a good approximation using adiabatic elimination of the other eigenstates. In this approximation, the central quantity is the overlap

$$\langle R | \hat{H} | L \rangle = \left| a_1 e^{-(N-1)/\xi} v_N b_N \right| e^{i\phi}, \quad (1.55)$$

with some $\phi \in [0, 2\pi)$. The energy eigenstates are approximated as

$$|0+\rangle = \frac{e^{-i\phi/2} |L\rangle + e^{i\phi/2} |R\rangle}{\sqrt{2}}; \quad E_+ = \left| a_1 e^{-(N-1)/\xi} v_N b_N \right|; \quad (1.56)$$

$$|0-\rangle = \frac{e^{-i\phi/2} |L\rangle - e^{i\phi/2} |R\rangle}{\sqrt{2}}; \quad E_- = - \left| a_1 e^{-(N-1)/\xi} v_N b_N \right|. \quad (1.57)$$

The energy of the hybridized states thus is exponentially small in the system size.

1.6 Summary

A one-dimensional chiral symmetric lattice insulator can have topologically protected zero-energy edge states at its ends, predicted by the winding number of the bulk.

Chiral symmetric lattice insulator:

- Each unit cell has an even number $2M$ sites.
- Each site belongs to sublattice A or B .
- Hamiltonian induces no transitions between sites on same sublattice, $\hat{P}_A \hat{H} \hat{P}_A = \hat{P}_B \hat{H} \hat{P}_B = 0$.

Edge states:

- wavefunction is localized at the edge, decaying exponentially towards the bulk;
- wavefunction has support on one sublattice only (opposite on opposite edges);
- energy is exponentially small in system size, $E \propto e^{-N/\xi}$.

Winding number:

- Defined for translation invariant bulk (alternative definitions for non-translation invariant case exist)

$$H(k) = \begin{pmatrix} 0 & h(k) \\ h^\dagger(k) & 0 \end{pmatrix}; \quad \nu = \frac{1}{2\pi i} \oint_{-\pi}^{\pi} dk \frac{d}{dk} \log \det h(k). \quad (1.58)$$

Simplest example is the SSH model, with $M = 1$.

$$\hat{H} = v \sum_{m=1}^N (|m, B\rangle \langle m, A| + h.c.) + w \sum_{m=1}^{N-1} (|m+1, A\rangle \langle m, B| + h.c.); \quad (1.59)$$

$$\hat{H}(k) = \underbrace{(v + w \cos k)}_{d_x} \hat{\sigma}_x + \underbrace{w \sin k}_{d_y} \hat{\sigma}_y; \quad h(k) = v + w e^{-ik}. \quad (1.60)$$

- trivial if $v > w$,
- topological if $v < w$.
- If topological: one topologically protected edge state on sublattice A at the left edge, on sublattice B at the right edge.
- winding number in this case: the winding of the endpoint of $(d_x(k), d_y(k))$.

Problems

Higher winding numbers

The SSH model is one-dimensional in space, and has a two-dimensional internal Hilbert space. Construct a lattice model that has these properties of the SSH model, but which has a bulk winding number of 2. Generalize the construction for an arbitrary integer bulk winding number.

Complex-valued hopping amplitudes

Generalize the SSH model in the following way. Assume that the hopping amplitudes

$v = |v|e^{i\phi_v}$ and $w = |w|e^{i\phi_w}$ are complex, and include a third complex-valued hopping amplitude $z = |z|e^{i\phi_z}$ between the states $|m, A\rangle$ and $|m+1, B\rangle$ for every m . Provide a specific example where the tuning of one of the phases changes the bulk winding number.

A possible generalization to two dimensions

Consider a two dimensional generalization of the SSH model. Take parallel copies of the SSH chain and couple them without breaking chiral symmetry. What will happen with the edge states?